The Assembly of Amyloidogenic Yeast Sup35 as Assessed by Scanning (Atomic) Force Microscopy: An Analogy to Linear Colloidal Aggregation?

Shaohua Xu,* Brooke Bevis,† and Morton F. Arnsdorf*
Departments of *Medicine and Molecular Genetics and †Cell Biology, The University of Chicago, Chicago, Illinois 60637 USA

ABSTRACT Amyloidosis is a class of diseases caused by protein aggregation and deposition in various tissues and organs. In this paper, a yeast amyloid-forming protein Sup35 was used as a model for understanding amyloid fiber formation. The dynamics of amyloid formation by Sup35 were studied with scanning force microscopy. We found that: 1) the assembly of Sup35 fibers begins with individual NM peptides that aggregate to form large beads or nucleation units which, in turn, form dimers, trimers, tetramers and longer linear assemblies appearing as a string of beads; 2) the morphology of the linear assemblies differ; and 3) fiber assembly suggests an analogy to the aggregation of colloidal particles. A dipole assembly model is proposed based on this analogy that will allow further experimental testing.

INTRODUCTION

The aggregation and deposition of biomolecules are believed to be the underlying cause of many human diseases, including atherosclerosis, amyloidosis, and stones in the gallbladder and kidney (Kumar et al., 1997). Amyloidosis, regardless of clinical syndrome and chemical diversity, is characterized by deposition of aggregated proteins and protein peptides in the form of fibrils in various tissues and organs (Costa et al., 1978; Husby 1992; Tan and Pepys, 1994). Nearly 80 peptides are reportedly amyloidogenic. They have little sequence homology, but can form fibers that can bind Congo red.

Understanding the mechanism of the amyloid fiber formation is of both medical and biological importance. An interesting issue is why these proteins aggregate linearly. In this experiment, we used a yeast amyloid-forming protein, Sup35, to study fiber assembly in vitro (Glover et al., 1997). Sup35 is a subunit of the translation termination factor. In some cases, however, the protein exists as an aggregate [PSI^+], which reduces its function and increases the read-through frequency of ribosomes over stop codons (Cox et al., 1998; Wickner 1994). The inheritable message of [PSI^+] is carried along by the altered protein structure rather than by nucleic acids, similar to the kind of propagation of the mammalian prions thought to be responsible for progressive, fatal neurodegenerative diseases including Creutzfeldt-Jacob disease, Kuru, and fatal familial insomnia in humans, scrapie in sheep, and "mad cow" disease.

Overexpression of the wild-type Sup35 protein induces both the [PSI+] phenotype and the heritable [PSI+] element, analogous to the overexpression of prion protein and prions. Transient overexpression is sufficient to convert [PSI^-] to [PSI^+], and the [PSI+] state is maintained even when the plasmid that confers overexpression is lost. Sup35 fibers formed in vitro bind with Congo red, and transmission electron microscopy (TEM) has revealed that most of the Sup35 fibers are long, smooth, semi-rigid rods (Glover et al., 1997).

Sup35 consists of 686 amino acid residues and is divided into three arbitrary regions by two Met residues (Fig. 1, amino acids 125 and 253) (Glover et al., 1997). The N terminus region (N, amino acids 1–124), which is rich in Gln, Asn, Gly, and Tyr, is required for [PSI^+] formation in vivo. The middle region (M, amino acids 125–253) is highly charged. In vivo, it facilitates [PSI^+] formation. The C-terminal region (C, amino acids 254–686) contains four GTP-binding sites and interacts with the partner protein Sup45 to provide the essential function of this protein in translation termination. Although the fiber-forming domain has been attributed to the amino-terminal 123 residues (N), it is difficult to capture the dynamic states of the polymerization of this peptide. Instead, we performed scanning (atomic) force microscopy (SFM) with a peptide consisting of the amino terminal 253 residues (NM, Glover et al., 1997).

SFM is a powerful tool in studying the structure and dynamics of assembly of macromolecules (Binnig et al., 1986; Hansma and Hoh, 1994; Lal and John, 1994, Czajkowsky and Shao, 1998; Xu, 1998). SFM has detected precursor protofibrils in the assembly of Aβ amyloid (Harper et al., 1999), small oligomeric forms of α-synuclein which may be analogous to the Aβ protofibril (Conway et al., 2000), and the bidirectional growth of protofibrils that developed into fibrillar amylin fibrils in vitro (Goldsbury et al., 1999). In this paper, we have captured images of NM fibers in various stages of formation. Our studies have revealed possible intermediates in the pathway to the formation of NM fibers including

Received for publication 27 October 2000 and in final form 4 April 2001.
Address reprint requests to Shaohua Xu, Ph.D., The University of Chicago, Department of Medicine, MC6080, 5841 S. Maryland Ave, Chicago, IL 60637. Tel.: 773-702-1086; Fax: 773-702-8875; E-mail: shxu@medicine.bsd.uchicago.edu.

0006-3495/01/07/446/09 $2.00

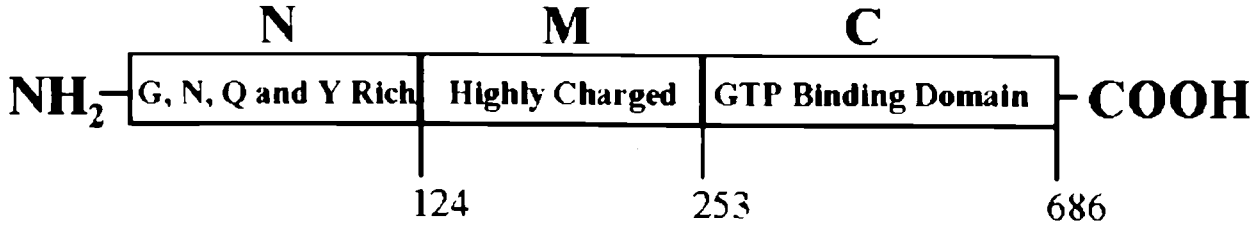

FIGURE 1 The three regions of Sup35. The N region, between residue 1 and 124, is rich in Gly, Tyr, Asn, and Gln. This region has a very low solubility in aqueous solution and is responsible for the fiber formation of the protein. The M region, between residue 125 and 253, is highly charged. This region facilitates [PSI^+] formation. The C region, between residue 253 and 686, consists of GTP-binding sites and is responsible for the function of Sup35 in translation termination. A peptide consisting of the N and M region is used in this study. This peptide is named NM.

individual NM peptides, large beads, and short fibers. Images show these intermediates assembling linearly, appearing as a string of beads. Additionally, we present a number of images of mature fibers that suggest possible interaction among fibers.

MATERIALS AND METHODS

SFM imaging

A NanoScope III AFM-1 was used in these experiments. We have described the method in detail (Xu and Arnsdorf, 1994). We routinely calibrate the instrument with mica to ensure accurate movement in the *x-y* plane. Imaging generally begins in a 5×5 nm^2 area. When stable images are obtained, the scanning force is minimized by a reduction of the set point voltage, and the scanning area is increased to the desired size. The raw data are plane-fit, which flattens a wavy image by calculating a single polynomial of a selectable order for the wavy image and then subtracting it from the image. The dimensions of the imaged molecules are measured with the NanoScope III off-line data analysis program by use of the section profile.

Selection and calibration of the SFM tip with colloidal gold particles

Colloidal gold particles were imaged with various cantilever tips. Those tips that generated round images of the gold particles with relatively small tip-induced broadening were used. The details of the calibration procedure have been published (Xu and Arnsdorf, 1994). Briefly, colloidal gold particles, with a diameter similar to that of the imaged molecules, were scanned with the tip both before and after imaging of the specimen. The sectional sizes of the gold particles at various image heights were analyzed, which allows derivation of the sectional radii at these image heights. The sectional radius is the sum of the sectional radius of the tip and that of the gold particle at each of the points on the particle touched by the tip. Thus, based on the measured sectional sizes of the image of the gold particle, one can derive the sectional radius of the tip at any point near the tip apex. When an image of a specimen was analyzed, the tip sectional radius was subtracted from the apparent sectional radius of the specimen to yield the actual size.

Fiber preparation

The NM peptide of Sup35 that contained a polyhistidine extension was prepared following the method by Glover et al. (1997). Briefly, cells were lysed by gentle agitation in urea solution (20 mM Tris-HCl, 8 M urea, pH 8.0) for 30 min. Insoluble material was pelleted by centrifugation at $30,000 \times g$ for 20 min. The supernatant was passed through an affinity column (Ni^{2+}-NTA agarose, 2.5 cm $\times$ 10 cm). Unbound proteins were rinsed off with the urea solution containing 40 mM imidazole. The NM peptides bound to the agarose beads were eluted with the urea solution containing 400 mM imidazole. Protein concentration was determined following the BCA micro assay method (Pierce, Rockford, IL). Concentrated NM solution (20 mg/ml in 20 mM Tris, 8 M urea, pH 8.0) was diluted 200-fold into phosphate buffer (10 mM sodium phosphate, 150 mM NaCl, pH 7.2). The reaction mixture was incubated at room temperature and an aliquot of sample (10 μl) was removed at designated time points for SFM analysis.

Specimen preparation for SFM imaging in air and in solution

An aliquot of protein, sufficient to form a layer on mica (1 cm in diameter), was mixed into phosphate solution pre-loaded on mica (10 mM sodium phosphate, 100 mM NaCl, pH 7.0). The specimen was incubated at room temperature for 5 min for adsorption of the protein to the surface of the mica. For imaging in solution, the specimen was then directly mounted onto the sample stage and imaged. Phosphate buffer was used as the imaging solution. For imaging in air, the mica disk was soaked in a weighing boat (diameter, 3 cm) filled with 5 ml of the phosphate solution for removal of unbound proteins, rinsed with 5 drops of water, and dried in air for at least 3 h before being imaged.

Statistical test

We analyzed the distribution of the particle heights and tested how many peaks were present. Shapiro-Wilk test statistics, or W statistics, were used (Shapiro and Wilk, 1965). We assumed a normal distribution of the measured heights of the particles. If a normal distribution was established, one peak was inferred. If the assumption was rejected, we applied a kernel density estimation to calculate the number of peaks present.

Limitations

The strength and limitations of SFM imaging have been considered in detail in our previous publications (Xu and Arnsdorf, 1994, 1997). The question could be raised that the dry samples could artifactually aggregate. We do not believe that this is a problem because wet samples had an appearance very similar to the dried samples (compare, for example, the images of the dried samples with that of a wet sample; see fig. 5 *D*). The

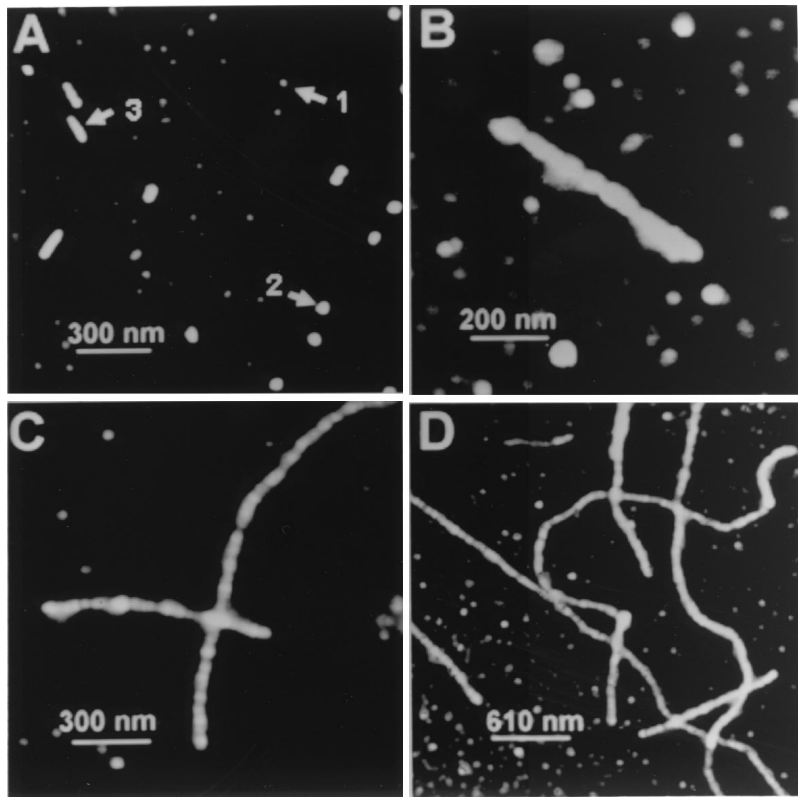

FIGURE 2 SFM images of fibers made from the NM peptides of Sup35 at different stages. Samples captured at various time points from the NM fiber formation reaction were deposited on mica and imaged with SFM in air. (*A*) was obtained at 2 h, and *B*, *C*, and *D* at 23 h. In *A*, small beads (1), the presumed individual NM peptides, and large beads (2), the presumed nucleation units, can be identified. Young fibers appearing as dimers, trimers, and tetramers of the large beads are also present in *A* (3). The fibers grew to intermediate length or longer at times 23 h or longer after initiation of the aggregation (*B–D*). These fibers also appear as strings of beads.

washing procedure before drying specimens seems adequate because we did not image any salt deposition on mica when a specimen was prepared in the absence of proteins.

RESULTS

Dynamics of Sup35 fiber formation

Samples captured from different stages of the reaction were analyzed with SFM and are presented in Fig. 2. Two hours after the initiation of the assembly reaction (Fig. 2 *A*), a mixture of small (presumably individual NM peptides) and large beads (presumably nucleation units), which, in turn, form dimers, trimers, tetramers, and longer linear assemblies appearing as a string of the large beads. We define the nucleation units as beads that are large enough for the linear assembly and formation of fibers. It appears to be the end stage of spherical aggregation as well, because the repeating units of the fiber have a lateral dimension equal to or larger than the diameter of the largest beads found, as will be discussed in detail. At 23 h (Fig. 2, *B–D*), fibers of intermediate length (in the range of 200–600 nm) and long fibers (>1 μm) were found. Fibers of all lengths appear to be chains of the large beads. This suggests that the large beads are nucleation units for fibers.

Formation of the nucleation units

Intermediates for nucleation unit formation were captured at the initial stage (2 h time point) of the fiber formation. Analysis of 325 beads reveals that the height of the beads distribute in two groups. The height of the small beads ranged between 3.4 and 6.0 nm ($n = 198$), distributing in one peak with a mean of 4.0 ± 1.1 nm (p1 in Fig. 3), which agrees with the predicted size of the NM peptides. The variation in height could reflect different orientations of the individual NM peptides on the surface of the mica. Some small beads, with heights less than 3.4 nm, may represent the degradation products of NM peptides.

Measured and calibrated lateral size of the nucleation units

The height of the large beads ranged between 10.6 and 17 nm, distributing bimodally with mean peaks of 14.1 nm and 16.1 nm (p2 and p3 in Fig. 3). These particles appear as various isoforms of nucleation units in their final stage of formation. No beads with heights between 6.0 and 10.6 nm were found.

The lateral size of the beads are overestimated because of the tip convolution effect. Calibration of the effect yields their true dimensions. We calibrated the tip con-

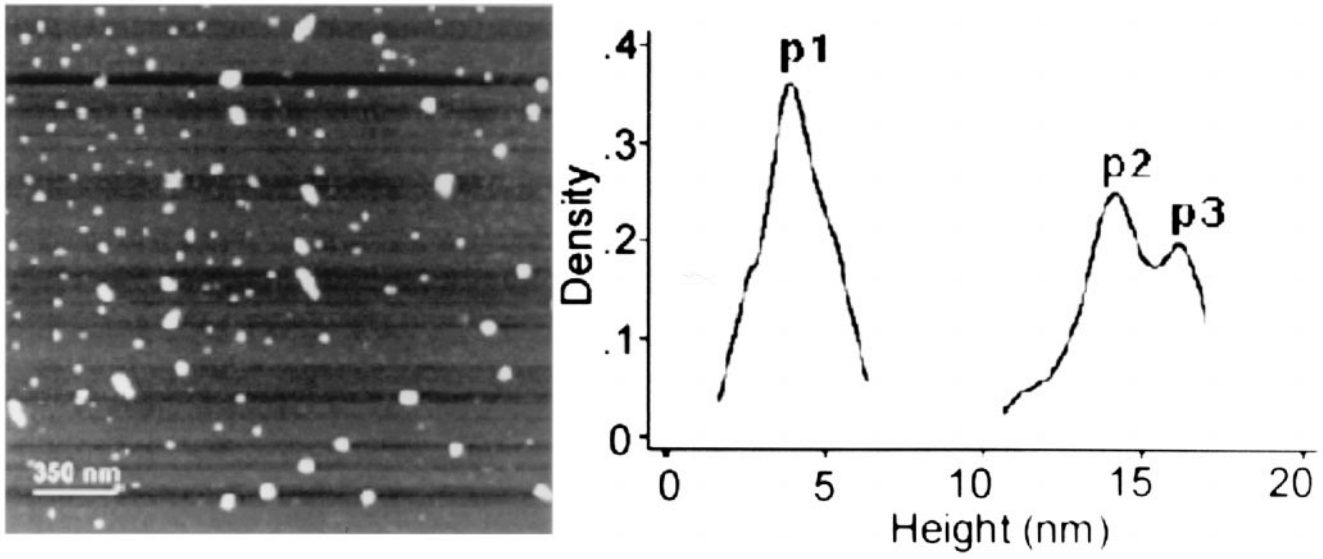

FIGURE 3 An SFM image of NM peptides in various aggregation states and height distribution of these aggregates at 2 h after initiation of the reaction. Peak p1 represents the pool of individual NM peptides (p1 = 4.0 nm) or the small beads. Peaks p2 and p3 (14.1 and 16.1 nm, respectively) represent populations of NM aggregates that are the large beads and are thought to be the nucleation units for the fibers.

volution effect by imaging the tip with colloidal gold particles first to determine its geometry (Xu and Arnsdorf, 1994, 1997). The height of individual gold particles can be imaged accurately and is used as the diameter of the particle for calibration of the tip convolution effect. The SFM tip, calibrated with 20 nm colloidal gold particles, has a radius of curvature of 21.6 nm, a semivertical angle of 38.6°, and a cutoff height of 13.0 nm. The diameter of the large beads (p3) were measured to be 69.8 ± 3.6 nm (apparent diameter, $n = 25$). The calibrated diameter, 31.2 ± 1.7 nm, is similar to the measured repeating unit of the fiber, 32.9 nm (see below). The same tip was used for the acquisition of images shown in Figs. 2–4.

Formation of fibers

The height measurements of a few young fibers are shown in Fig. 4. These heights varied between 8.8 and 16.5 nm, possibly depending on the size of the nucleation units assembled. The dimers were taller than the trimers and tetramers. The height of the nucleation units along a single fiber varied as well, as shown for the trimer (Fig. 4 *A*). The dimer shown has a measured height of 14.5 nm, and the trimer has various heights for different nucleation units, measured to be 8.8, 11.0, and 12.3 nm.

Fibers from samples collected 20 h after the initiation of the polymerization had a mean measured height of 14.1 ± 2.7 nm ($n = 38$), which varied from bead to bead on the same or different fibers in a range from 9.0 to 18.9 nm. Although the height varied, there was a tendency for a fiber to be made of nucleation units of similar diameters (data not shown).

Length of the repeating unit of the young and mature fibers

Young fibers consisting of two, three, or four nucleation units were found (Fig. 4 *A*). The center-to-center distance between neighboring nucleation units in these young fibers was consistently measured to be 32.9 nm (Fig. 4, representative measurement a_3 to a_4), indicating this is the repeating unit for the young fibers. The length of the dimers, measured between a_1 and a_2, was 102.0 nm, which is larger than twice the repeating unit 65.8 nm (2×32.9 nm). The difference between 102.0 nm and 65.8 nm, 36.2 nm, is the overestimation of the lateral dimension due to the tip convolution effect for the two ends of the fibers. When the convolution effect is considered, the measured length of the trimer (b_1b_2: 134.8 nm) agrees with the predicted length of a trimer with a repeating unit 32.9 nm, $3 \times 32.9 + 36.2 = 134.8$ nm. Similarly, the measured length of the tetramer (c_1c_2: 164.4 nm) was very close to the predicted length of a tetramer with periodicity of 32.9 nm, $4 \times 32.9 + 36.2 = 167.8$ nm. Surprisingly, the repeating unit in the mature fibers, d_1d_2, was measured to be 61.1 ± 10.1 nm ($n = 50$, *B*), almost twice as large as the repeating unit of the young fibers but less homogeneous. This diversity suggests continuous structural changes as the fibers age.

The measured height for the young fibers, ranging from 8.8 to 16.5 nm, overlaps with the height found for

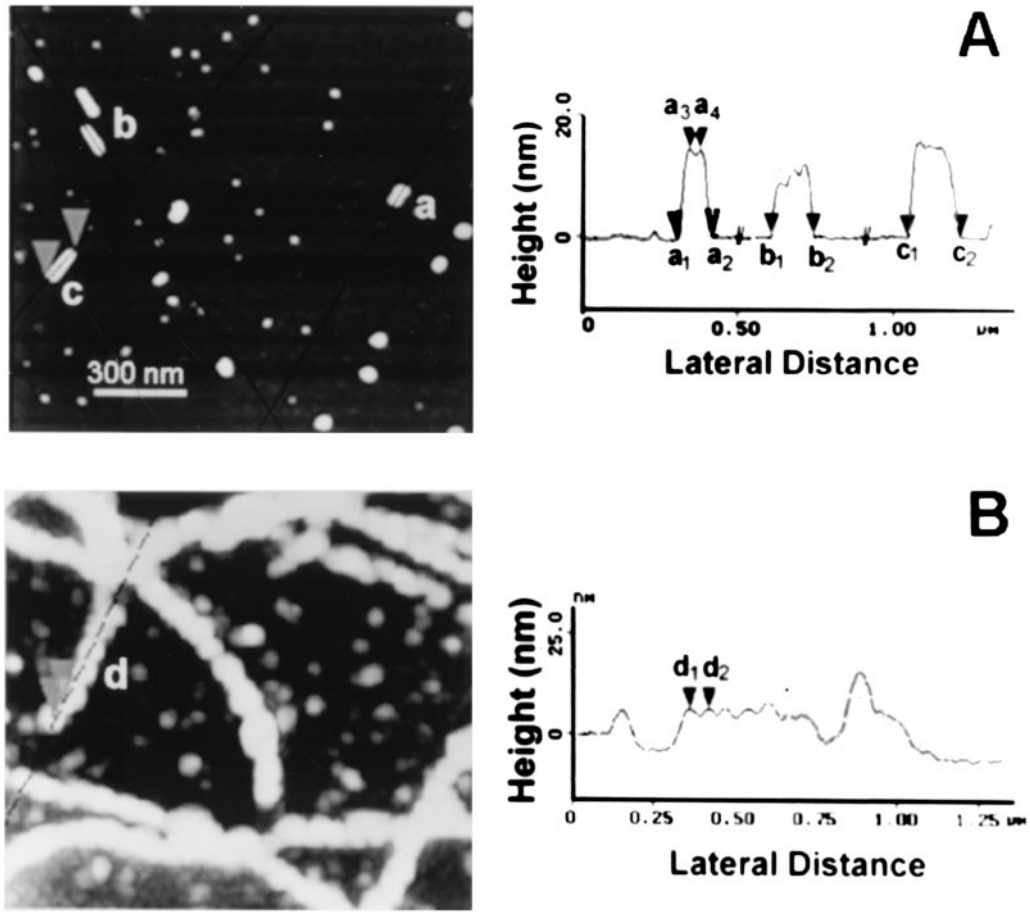

FIGURE 4 The length of the repeating unit of the young and mature fibers. (*A*) The young fibers made of two, three, and four of the nucleation units were analyzed for their lateral dimensions. The dimensions were determined using the section analysis program of the Nanoscope III software. The repeating unit of the young fibers was 32.9 nm (a_3a_4). The difference between a_1a_2 and $2 \times a_3a_4$ is regarded as the tip-induced convolution (36.2 nm). When the convolution effect is considered, the measured length of the trimer (b_1b_2: 134.8 nm) and tetramer (c_1c_2: 167.8 nm) agrees with the predicted length of a trimer and a tetramer. (*B*) The repeating unit of the mature fibers was 61.1 ± 10.1 nm (d_1d_2). The images presented were acquired in air. The scale of 300 nm is for both images.

the large beads, 10.6 to 17.0 nm. This size similarity suggests that these beads are the actual nucleation units of the fibers. On the other hand, these numbers are much smaller than the lateral diameter of the large beads, 31.2 nm (after calibration for tip convolution effect), and the lateral repeating units of the young fibers, 32.9 nm, further suggesting structural changes as the nucleation units aggregate linearly.

The number of NM peptides needed for the formation of the nucleation units can be estimated. If one assumes the NM peptides and the nucleation units have the same compressibility and the nucleation unit is close-packed (either face-centered or body-centered), then, the number of NM peptides in each nucleation unit can be estimated as: $(V_{\text{nucleation}}/V_{\text{NM peptide}}) \times 0.74 = (4/3\pi r_{3\text{nucleation}})/(4/3\pi r^3_{\text{NM peptide}}) \times 0.74$, where $V_{\text{nucleation}}$ and $V_{\text{NM peptide}}$ are the respective volumes of the beads; $r_{\text{nucleation}}$ and $r_{\text{NM peptide}}$ are the radius of the beads and the NM peptides, and 0.74 is the factor of maximum packing density (Howe, 1997). We estimate the number of NM peptides in a nucleation unit to be between 32 and 48, using values of 14.1 and 16.1 nm for the diameters of the nucleation units and 4.0 nm for the NM peptides (p2, p3, and p1 in Fig. 3).

Interaction among mature fibers

Fibers found in samples collected 50 h after the initiation of the polymerization are shown in Fig. 5. Most fibers appear straight, but some fibers seem to branch (Fig. 5 *A*) while others have a zig-zag appearance (1 in Fig. 5 *B*). The width and length varies from one mature fiber to another. Mature fibers can twist around each other (1 and 2 in Fig. 5 *C*) and, at times, develop a side by side orientation (Fig. 5 *D*). These complicated morphologies are only observed in mature fibers.

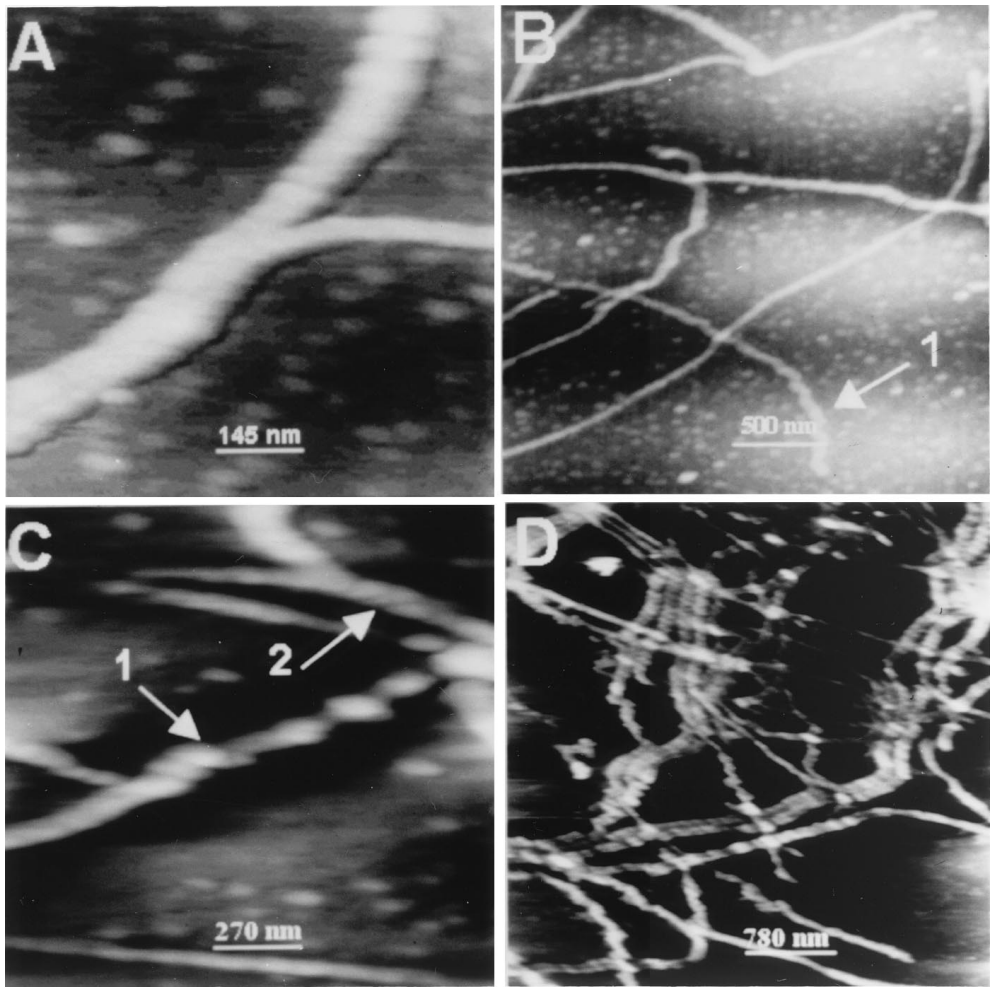

FIGURE 5 Interaction between mature fibers. The reaction mixture at 50 h was deposited on mica and imaged in air (*A–C*) and in phosphate solution (*D*; 10 mM sodium phosphate, 150 mM NaCl, pH 7.4). Branching (*A*), zig-zag (1 in *B*), twisting (1 and 2 in *C*), and side to side interactions between fibers (*D*) are seen in these images. Also, some fibers become wider near the end (1 in *B*).

DISCUSSION

The dynamic states of Sup35 polymerization were captured and visualized with SFM. The images and the size analysis show that the individual NM peptides of Sup35, appearing as small beads, seem to fuse and form large beads or what we have termed nucleation units. The nucleation units, in turn, probably chain together and form fibers. The fiber assembly process appears analogous to the aggregation of colloidal particles in the presence of an intrinsic or induced dipole moment (Winslow, 1949; Adriani and Gast, 1990; Halsey, 1993; Halsey et al., 1997). Colloidal aggregation involves two steps: the formation of nucleation units and the aggregation of nucleation units (Jullien and Botet, 1987). Based on these results and analysis, we provide a dipole assembly model for the Sup35 fiber formation that may be generalizable to other amyloid fibers.

Quantitative analysis indicates that the nucleation units of various sizes are found in the young fibers formed early in the reaction. Based on analysis of the measured heights of the individual NM peptides (p1) and the nucleation units (p2 and p3), the number of NM peptides needed to form a nucleation unit is estimated to be between 32 to 48. The mature fibers retain the appearance of a string of beads, but are larger in diameter and in lateral repeating units than the young fibers. These mature fibers can twist around each other or bind together side by side. Various types of assembly were observed including branching and zig-zag formation.

Formation of a nucleation unit from individual NM peptides could result from decreased protein solubility following reduction of the urea concentration. The NM peptides may misfold upon dilution of urea, exposing hydrophobic regions to the aqueous solvent. Hydrophobic interactions such as these could cause the misfolded

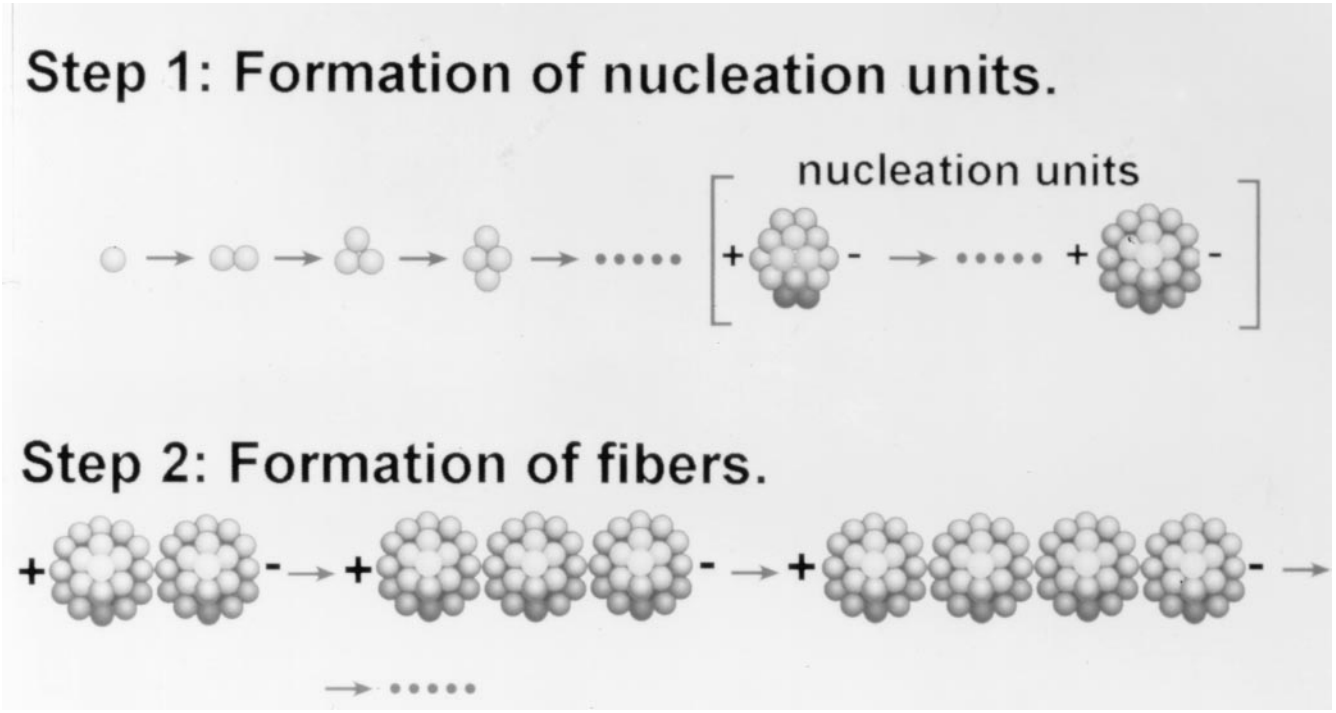

FIGURE 6 Model for Sup35 fiber formation. Driven possibly by hydrophobic interactions, misfolded NM peptides aggregate and form nucleation units (Step 1). The nucleation units may have an intrinsic dipole moment and thus aggregate linearly forming amyloid fibers (Step 2). Nucleation units of similar and/or different sizes seem capable of assembling together and forming fibers. The size of the nucleation units might be determined by the magnitude of the dipole moment needed to overcome repelling force between the nucleation units or between the nucleation unit and a fiber. The integrative dipole moment of a fiber may enable the fiber to behave like a template attracting new nucleation units to the ends of the fibers. Although not illustrated in the model, continuous structural changes seem likely, including fusion of neighboring nucleation units, resulting in mature fibers with increased lateral repeating units and decreased heights.

NM peptides to aggregate and form nucleation units. If these nucleation units have dipole moments, the attractive force between dipoles could account for the linear assembly of the nucleation units. Of the 253 residues in the NM peptide, 24% are charged. The N-terminal region of the NM peptide is less polar and less charged than the M region. The N region is rich in two helix-breaking residues, Gly and Pro, and two nonpolar aromatic residues, Tyr and Phe. The M region is rich in two polar residues, Ser and Thr, and the charged residues, Glu, Asp and Lys. It has been shown that the N region alone aggregates rapidly in the absence of urea (Glover et al., 1997). This suggests that the N region may contribute more to the hydrophobic induced aggregation and spherical nucleation unit formation and the M region may contribute to the initial columbic repelling force and the subsequent dipole-dipole interaction. This repelling force may prevent the unlimited growth of individual nucleation units. These asymmetrically distributed charges may also drive the dipole-dipole interaction, leading to the linear aggregation of the nucleation units and the formation of the fibers.

If this hypothesis is correct, the high concentration of charged residues may be responsible for the intrinsic or induced dipole moment of the nucleation unit. We suspect that the dipole moment of a nucleation unit would increase as more NM peptides aggregate. Once the dipole-dipole interaction is strong enough to overcome the thermal energy and the electrostatic repulsion between the nucleation units, linear aggregation of the nucleation units would occur (Fig. 6). As the fibers become longer, the integrative dipole moment will increase and then level off. The integrative dipole moment of a fiber would exercise a stronger attractive force than a nucleation unit to another nucleation unit, therefore causing exponential fiber growth. Thus, pre-formed fibers may serve as a template and facilitate the addition of free nucleation units to the end of the fibers via the dipole-dipole attraction.

This dipole assembly model may explain a number of intriguing properties of amyloid fibers and amyloidosis that have previously been puzzling. We explained the template phenomena in the last paragraph. A similar explanation could also be applied to seeding, a process that eliminates the lag time in fiber formation. According to the dipole assembly model, seeding could provide fibers with strong integrative dipole moments. The strong dipole moment of the fiber seeds may facilitate the as-

sembly of new nucleation units to the fiber, either by inducing a dipole in the nucleation units or by attracting already polarized nucleation units, thereby promoting fiber elongation.

The dipole assembly model sets little restriction on the size of the nucleation units. Various amyloid fibers are known to have significantly different diameters. According to the dipole assembly model, the primary driving force for assembly would be dipole moment strength rather than physical size. Linear aggregation would occur between two nucleation units once their dipole-dipole interaction was strong enough to overcome the repelling forces between them. Furthermore, colloidal particles of different sizes are known to align in an electric field due to the induced dipole-dipole interaction between these particles (Halsey, 1993).

Of the over 80 amyloid forming peptides, there is little sequence homology, but they all have a significant number of charged residues (Tan and Pepys, 1994). Our model proposes two steps to amyloid fiber formation. The first step is driven by hydrophobic interactions which require little or no sequence homology. The second step is driven by dipole-dipole interaction, which requires charged residues but not sequence homology.

Our model is similar in some respects to proposals from other laboratories. The preformed amyloid is thought to be able to catalyze the conversion of the soluble conformers to conformations that give rise to the aggregates (Tuite and Lindquist, 1996). We believe that the native and the misfolded conformers exist in solution in a quasi-equilibrium state. The preformed fibers could shift the balance by promoting the formation of nucleation units from the misfolded conformers as if they were catalyzing the conversion of the native conformer to the misfolded ones. Jarret and Landsbury (1993) proposed the idea of nucleation-dependent polymerization of amyloid fibers. They suggested that following nucleation, the elongation of fibers occurs by the addition of single peptides to the fibers. Our model is in agreement with the initiation of fiber formation being dependent on a nucleation event. However, we believe that elongation of the fibers is a process of linear aggregation of preformed nucleation units. Our model does not eliminate the possibility of addition of single peptides to preformed fibers as a supplementary pathway for fibers to grow longer and wider.

To validate the dipole assembly model, it is critical to test the behavior of the fibers under an electric field. If the aggregation of nucleation units is driven by dipole interactions and the pre-formed fibers have an integrative dipole moment, these fibers should line up with an external electric field (Adriani and Gast, 1990). The strength of the electric field needed to observe such phenomena would allow an estimate the strength of the integrative dipole moments of short and long fibers.

This work was supported by the University of Chicago-Argonne National Laboratory Collaborative grant Programs (S.X.), by National Institutes of Health GM57840 (to M.F.A), and by R44GM/HL56056 (M. Griem, PI, Subcontract to M.F.A. and S.X.).We thank Drs. Ming Zhang and Duan P. Chen for helpful discussions. We thank Dr. Susan Lindquist's laboratory for providing the NM peptides.

REFERENCES

Adriani, P. M., and A. P. Gast. 1990. Electric-field-induced aggregation in dilute colloidal suspensions. *Faraday Discuss.* 90:17–29.

Binnig, G., C. F. Quate, and C. Gerber. 1986. Atomic force microscopy. *Phys. Rev. Lett.* 56:930–933.

Conway, K. A., J. D. Harper, and P. T. Lansbury, Jr. 2000. Fibrils formed in vitro from alpha-synuclein and two mutant forms linked to Parkinson's disease are typical amyloid. *Biochemistry.* 39:2552–2563.

Costa, P. P., A. S. Figueira, and F. R. Bravo. 1978. Amyloid fibril protein related to prealbumin in familial amyloidoitic polyneuropathy. *Proc. Natl. Acad. Sci. U.S.A.* 75:4499–4503.

Cox, B. S., M. F. Tuite, and C. S. McLaughlin. 1998. The psi factor of yeast: a problem in inheritance. *Yeast.* 4:159–178.

Czajkowsky, D. M., and Z. Shao. 1998. Submolecular resolution of single macromolecules with atomic force microscopy. *FEBS Lett.* 430:51–54.

Glover, J. R., A. S. Kowal, E. C. Schirmer, M. M. Patino, J. Liu, and S. Lindquist. 1997. Self-seeded fibers formed by Sup35, the protein determinant of [PSI^+], a heritable prion-like factor of S. cerevisiae. *Cell.* 89:811–819.

Goldsbury, C., J. Kistler, U. Aebi, T. Arvinte, and G. J. Cooper. 1999. Watching amyloid fibrils grow by time-lapse atomic force microscopy. *J. Mol. Biol.* 285:33–39.

Halsey, T. C. 1993. Electrorheological fluids-structure and dynamics. *Adv. Materials.* 5:711–718.

Halsey, T. C., B. Duplantier, and K. Honda. 1997. Multifractal dimensions and their fluctuations in diffusion-limited aggregation. *Phys. Rev. Lett.* 78:1719–1722.

Hansma, H. G., and J. H. Hoh. 1994. Biomolecular imaging with the atomic force microscope. *Annu. Rev. Biophys. Biomol. Struct.* 23: 115–139.

Harper, J. D., and P. T. Lansbury, Jr. 1997. Models of amyloid seeding in Alzheimer's disease and scrapie: mechanistic truths and physiological consequences of the time-dependent solubility of amyloid proteins. *Annu. Rev. Biochem.* 66:385–407.

Harper, J. D., S. S. Wong, C. M. Lieber, C. M., and P. T. Lansbury, Jr. 1999. Assembly of A beta amyloid protofibrils: an in vitro model for a possible early event in Alzheimer's disease. *Biochemistry*. 38: 8972–8980.

Howe, J. M. 1997. Interfaces in Materials. Ch. 8, Wiley-Interscience Publication.

Husby G. 1992. Amyloidosis. *Semin. Arthritis Rheum.* 22:67–82.

Jarrett, J. T., and P. T. Lansbury, Jr. 1993. Seeding one-dimensional crystallization of amyloid: a pathogenic mechanism in Alzheimer's disease and scrapie? *Cell.* 73:1055–1058.

Jullien, R., and R. Botet, Eds. 1987.Aggregates and Fractal Aggregates. Ch. 1. World Scientific Publishing Co., Singapore.

Kumar, V., R. S. Cotran, and S. L. Robbins. 1997. Basic Pathology. Ch.10, 14, and 16.

Lal, R., and S. A. John. 1994. Biological applications of atomic force microscopy. *Am. J. Physiol.* 266:C1–C21.

Shapiro, S., and M. B. Wilk. 1965. An analysis of variance test for nomality. *Biometrika.* 52:591–611.

Tan, S. Y., and M. B. Pepys. 1994. Amyloidosis. *Histopathology.* 25: 403–414.

Tuite, M. T., and S. Lindquist. 1996. Maintenance and inheritance of yeast prions. *Trends Genet.* 12:465–471.

Wickner, R. B. 1994. [URE3] as an altered URE2 protein: evidence for a prion analog in Saccharomyces cerevisiae. *Science*. 264:566–569.

Xu, S., and M. F. Arnsdorf. 1994. Calibration of the scanning (atomic) force microscope with gold particles. *J. Microscopy*. 173:199–210.

Xu, S., and M. F. Arnsdorf. 1997. Scanning (atomic) force microscopy imaging of earthworm haemoglobin calibrated with spherical colloidal gold particles. *J. Microscopy*. 187:43–53.

Xu, S. 1998. Apolipoprotein(a) binds to low-density lipoprotein at two distant sites in lipoprotein(a). *Biochemistry*. 37:9284–9294.

Winslow, W. 1949. Induced fibration of suspensions. *J. Appl. Phys.* 20: 1137–1145.